Developmental Cell
Article

Failure of Epithelial Tube Maintenance Causes Hydrocephalus and Renal Cysts in *Dlg5*$^{-/-}$ Mice

Tamilla Nechiporuk,[1] Tania E. Fernandez,[1] and Valeri Vasioukhin[1,2,*]
[1]Division of Human Biology, Fred Hutchinson Cancer Research Center, Seattle, WA 98109, USA
[2]Department of Pathology and Institute for Stem Cell and Regenerative Medicine, University of Washington, Seattle, WA 98195, USA
*Correspondence: vvasiouk@fhcrc.org
DOI 10.1016/j.devcel.2007.07.017

SUMMARY

Epithelial tubes represent fundamental building blocks of metazoan organisms; however, the mechanisms responsible for their formation and maintenance are not well understood. Here, we show that the evolutionarily conserved coiled-coil MAGUK protein Dlg5 is required for epithelial tube maintenance in mammalian brain and kidneys. We demonstrate that *Dlg5*$^{-/-}$ mice develop fully penetrant hydrocephalus and kidney cysts caused by a deficiency in membrane delivery of cadherin-catenin adhesion complexes and loss of cell polarity. Dlg5 travels with cadherin-containing vesicles and binds to syntaxin 4, a t-SNARE protein that regulates fusion of transport vesicles with the lateral membrane domain. We propose that Dlg5 functions in plasma membrane delivery of cadherins by linking cadherin-containing transport vesicles with the t-SNARE targeting complex. These findings show that *Dlg5* is causally involved in hydrocephalus and renal cysts and reveal that targeted membrane delivery of cadherin-catenin adhesion complexes is critical for cell polarity and epithelial tube maintenance.

INTRODUCTION

Multicellular organisms contain a variety of epithelial and endothelial tubes that are used to channel the passage of liquids and gases. These tubes vary in size and shape, but they share central building principles. They are made by highly polarized cells with distinct basal, lateral, and apical membrane domains. Defects in tube formation and maintenance are responsible for multiple human diseases, including obstructive hydrocephalus, kidney cysts, aneurysms, and vaso-inclusive diseases. Despite the fundamental importance of tubes in human biology, the mechanisms responsible for tube formation and maintenance are only now beginning to be understood (Lubarsky and Krasnow, 2003).

Mammalian Dlg5/P-Dlg is a PDZ-containing (PSD-95, Dlg, ZO-1) MAGUK (membrane-associated guanylate kinase) protein with homology to *Drosophila* neoplastic tumor-suppressor discs large (*dlg*). Sequence variation in human *DLG5* was initially reported to associate with inflammatory bowel disease; however, this association was not observed in some subsequent studies (Buning et al., 2006; Stoll et al., 2004). Based on sequence similarity, it has been proposed that *Dlg5* is another vertebrate homolog of *Drosophila dlg*; hence, the gene was named *Dlg5* (Nakamura et al., 1998). Here, we show that *Dlg5* is distinct from the Dlg family and is an evolutionary conserved gene with orthologs throughout the animal kingdom. We report that Dlg5 is necessary for the maintenance of epithelial tubes, and *Dlg5*$^{-/-}$ mice develop fully penetrant obstructive hydrocephalus and renal cysts. We reveal that, on the cellular level, brain and kidney abnormalities in *Dlg5*$^{-/-}$ mice result from the loss of cell polarity in the neural progenitor cells and epithelial cells lining the kidney collecting ducts. In addition, we report that, on the molecular level, Dlg5 is required for efficient delivery and stabilization of cadherin-catenin adhesion complex at the plasma membrane, and interaction between Dlg5 and t-SNARE membrane targeting complex may be responsible for these functions.

RESULTS

Dlg5 Is Distinct from the *Dlg* Family and Is an Evolutionarily Conserved Gene

To determine the expression pattern of Dlg5, we performed northern blot analyses (Figure 1A and data not shown). A single *Dlg5* transcript was expressed in multiple organs. The 7.8 kb size of Dlg5 mRNA was significantly larger than the originally published Dlg5 sequence (Nakamura et al., 1998). Analyses of mouse and human genome sequences revealed high-similarity regions located upstream from *Dlg5*. We confirmed the presence of an additional coding exon in the Dlg5 sequence by using RT-PCR and northern blot experiments (data not shown). This exon of Dlg5 had an ATG surrounded by a strong Kozak consensus sequence and was coding for the N-terminal CARD domain. Thus, the complete mouse Dlg5 cDNA encodes a large protein containing the CARD, Duff, coiled-coil, four PDZs, SH3, and GUK domains (Figure 1B, GB# AK147699).

Blast analyses revealed orthologous *Dlg5* genes in evolutionary distant species, such as *Drosophila melanogaster* (GB# NM_135661); zebra fish, *Danio rerio* (GB# XP_697520.1); and chicken, *Gallus gallus* (GB# XP_421604.1) (Figure 1B). The size and domain organization of Dlg5 differ

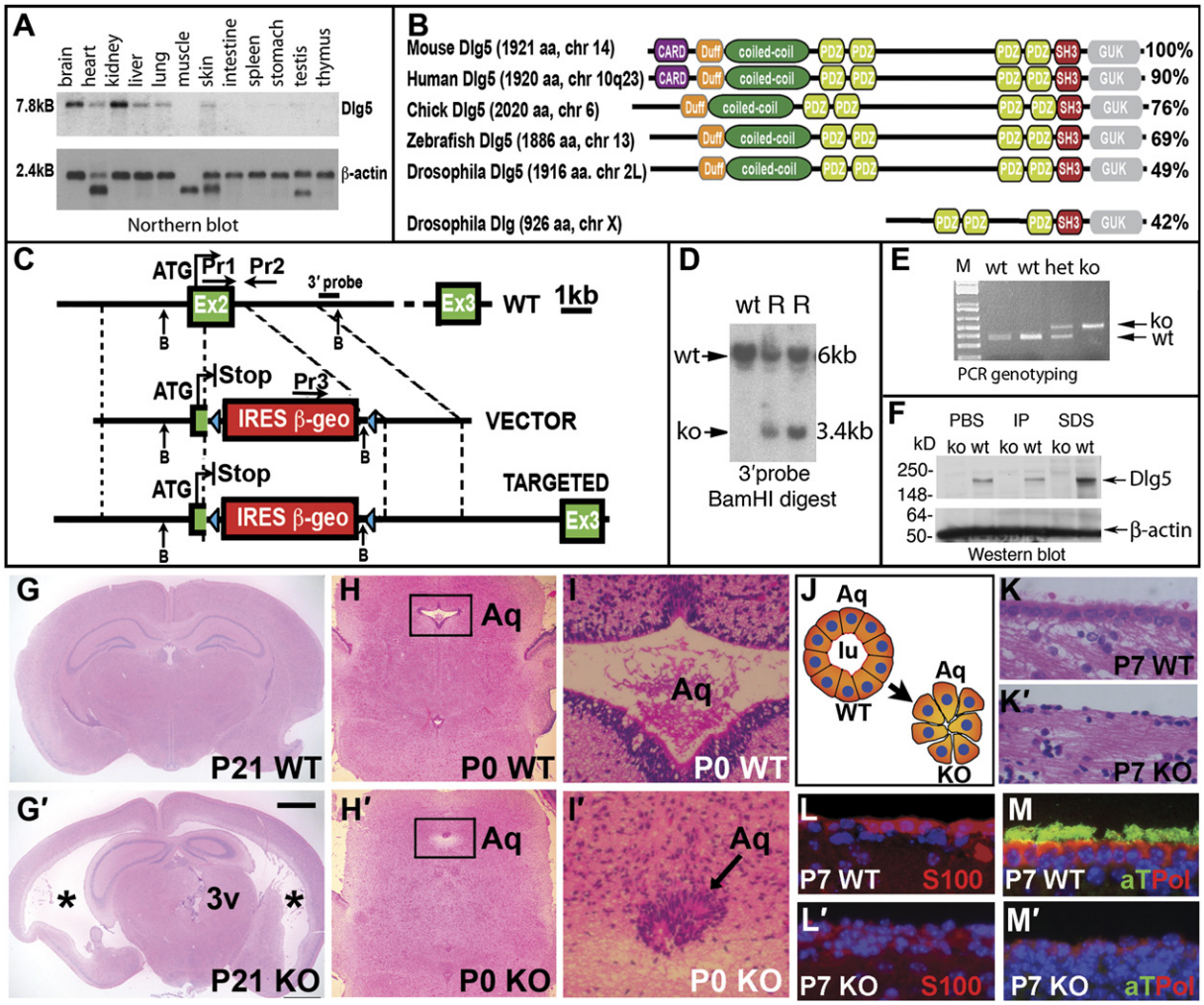

Figure 1. Fusion of the Aqueduct, Failure of Ependymal Cell Differentiation, and Severe Hydrocephalus in *Dlg5*$^{-/-}$ Mice

(A) The expression pattern of *Dlg5* in adult mouse organs. Northern blot analysis with *Dlg5* and *β-actin* probes.

(B) The domain organization of mouse, human, chick, zebrafish, and *Drosophila* Dlg5 proteins and *Drosophila* Dlg. The numbers on the right denote the percent similarity between mouse Dlg5 and Dlg5 in other species.

(C) Generation of *Dlg5* knockout mice. Schematic representation of the wild-type (WT) allele, targeting vector (VECTOR), and the resulting targeted allele (TARGETED). ATG indicates the initiating methionine in exon 2.

(D) Southern blot analyses of wild-type (wt) and targeted (ko) ES clones with the 3′ probe outside the targeting construct.

(E) PCR amplification of wild-type and knockout alleles from heterozygous (het) and knockout (ko) mice with primers 1, 2, and 3, shown in (C).

(F) Western blot analyses of proteins extracted from P7 brains of *Dlg5*$^{-/-}$ and wild-type animals by using sequential extraction with phosphate-buffered saline (PBS), 1% Triton X-100 buffer (IP), and 1% SDS. The blot was analyzed with anti-Dlg5 and anti-β-actin antibodies.

(G and G′) Haematoxylin and eosin (H&E) staining of coronal hippocampal sections from P21 wild-type (WT) and *Dlg5*$^{-/-}$ (KO) brains. Note the severe dilation of the lateral ventricles in the *Dlg5*$^{-/-}$ brain (asterisks) and disorganization of the third ventricle (3v).

(H–I′) H&E staining of P0 coronal brain sections at the level of the aqueduct. Boxed areas containing the aqueduct in (H) and (H′) are shown at higher magnification in (I) and (I′). Note the closure of the aqueduct (Aq, arrow) in *Dlg5*$^{-/-}$ mice.

(J) Model of the ventricular tube defect in *Dlg5*$^{-/-}$ brains. The apical surfaces of cells forming the tube are facing the lumen (lu).

(K–M′) Lateral ventricular surfaces from P7 mice stained with (K and K′) H&E, (L and L′) anti-S100 (ependymal cell marker), and (M and M′) anti-acetylated tubulin (aT, green, cilia marker), and polaris (Pol, red) antibodies. DAPI (blue) in (L)–(M′) stains cell nuclei. Note the absence of ciliated ependymal cells in the *Dlg5*$^{-/-}$ brain.

The scale bar in (G′) represents 1 mm in (G) and (G′), 0.4 mm in (H) and (H′), 70 μm in (K) and (K′), and 40 μm in (L)–(M′).

from those of classic Dlg family proteins, which are devoid of the N-terminal CARD, Duff, and coiled-coil domains. Thus, we conclude that Dlg5 is a unique and evolutionarily conserved protein. Evolutionary conservation of Dlg5 suggests a unique and important function.

Generation of *Dlg5* Knockout Mice

Dlg5 is an evolutionarily conserved gene; however, its in vivo function is unknown, since no organisms with a mutation in *Dlg5* have been previously generated and characterized. To reveal the functional role of *Dlg5*, we generated

Dlg5 knockout mice (Figures 1C–1F). Exon 2 was disrupted with the IRES-β-geo-polyA cassette, creating a stop codon after the first 25 amino acids of Dlg5, which lacked any functional domains. Western and northern blot analyses showed complete absence of the Dlg5 protein and mRNA in these mice (Figure 1F and data not shown). We concluded that we generated mice with the null allele of *Dlg5*.

Closure of the Aqueduct Leads to Severe Hydrocephalus in *Dlg5*$^{-/-}$ Brains

Although *Dlg5*$^{+/-}$ mice appeared to be indistinguishable from their wild-type counterparts, *Dlg5*$^{-/-}$ mice displayed growth retardation (Figure S1; see Supplemental Data available with this article online). The mutant pups developed a characteristic dome-like appearance of their heads. Histological analyses of *Dlg5*$^{-/-}$ brains revealed fully penetrant hydrocephalus (n = 20) with severe disorganization of the third brain ventricle and massive dilation and fusion of the lateral brain ventricles (Figures 1G and 1G′; Figure S2). The surviving adult *Dlg5*$^{-/-}$ mice developed a hopping gait (Movie S1), similar to hydrocephalic *hyh* mice (Chae et al., 2004).

To determine the cellular defect responsible for hydrocephalus, we performed a histological survey of newborn *Dlg5*$^{-/-}$ brains. Aqueduct of Sylvius, a tube connecting the third and fourth ventricles of the brain, was closed in postnatal day 0 (P0) *Dlg5*$^{-/-}$ brains (Figures 1H–1I′) (n = 6). While the cells lining the aqueduct were well organized in the wild-type mice, they were disorganized and failed to keep the aqueduct open in *Dlg5*$^{-/-}$ brains (Figures 1I–1J). We conclude that the closure of the aqueduct is responsible for hydrocephalus in *Dlg5*$^{-/-}$ mice. Thus, Dlg5 is necessary for the maintenance of the epithelial tube and ventricular lining in the mammalian brain.

Hydrocephalus in *Dlg5*$^{-/-}$ Brains Is Accompanied by Loss of Ependymal Cells and Disorganization of the Subventricular Stem Cell Niche

Ependymal cells form a continuous layer of multiciliated cells lining the ventricles (Spassky et al., 2005). Loss of ependymal cells, or denudation, can accompany hydrocephalus of various etiologies (Page and Leure-duPree, 1983; Sarnat, 1995). To study ependymal cells in *Dlg5*$^{-/-}$ brains, we analyzed the ventricular surface of P7 mice by using histology and markers of ependymal cells (S100) and cilia (acetylated tubulin and polaris). While cuboidal, multiciliated cells expressing S100, acetylated tubulin, and polaris were present on the surface of the wild-type ventricles, these cells were absent in *Dlg5*$^{-/-}$ brains (Figures 1K–1M′). Therefore, *Dlg5* is required for the formation of ependymal cells, and the ventricular surface is denuded in *Dlg5*$^{-/-}$ brains. Denudation of the ventricular lining may disturb the normal flow of cerebrospinal fluid and contribute to hydrocephalus in *Dlg5*$^{-/-}$ brains.

Histological analyses of lateral ventricles from P7–P21 *Dlg5*$^{-/-}$ brains revealed foci of abnormal cell accumulation, randomly distributed along the ventricular surface (Figures S3A–S3C′). These foci contained a heterogeneous population of proliferating cells expressing glial fibrillary acidic protein, GFAP (stem cell and astrocyte marker [Garcia et al., 2004]), Dcx2 (transient-amplifying cell marker [Doetsch et al., 2002]), and nestin (neural progenitor cell marker [Lendahl et al., 1990]) and did not express ependymal cell marker S100 (Figures S3D–S3J′). The cell-type-specific staining pattern and histology of dysplastic foci of *Dlg5*$^{-/-}$ brains were remarkably similar to those of the stem cell niche in the subventricular zone in wild-type brains. We conclude that, in the absence of the ependymal cell layer in *Dlg5*$^{-/-}$ brains, cells in the subventricular zone become disorganized and form dysplastic foci.

Disruption of Epithelial Cell Polarity, Loss of Cilia, and Kidney Cysts in *Dlg5*$^{-/-}$ Mice

In addition to tube maintenance defects in the brain, *Dlg5*$^{-/-}$ mice displayed severe epithelial tube maintenance defects in kidneys. Histological examination of *Dlg5*$^{-/-}$ kidneys revealed the formation of renal cysts (Figures 2A and 2A′). The phenotype was fully penetrant and varied from small cyst-like structures to large fluid-filled cysts. The large cysts were not lined by the polarized epithelial layer, but instead displayed a fibrous surface (inset in Figure 2A′). The blood urea nitrogen (BUN) levels were significantly higher in the mutant mice, suggesting impaired kidney function (Figure 2B). Whereas newborn *Dlg5*$^{-/-}$ kidneys were histologically undistinguishable from their wild-type counterparts, we observed dilations in kidney collecting ducts in the pelvis of P3 *Dlg5*$^{-/-}$ kidneys (Figures 2E and 2E′). Immunostaining with cell-type-specific markers revealed that the majority of cysts in *Dlg5*$^{-/-}$ kidneys were of collecting duct origin (Figures 2C and 2D). Interestingly, we found that collecting ducts express high levels of Dlg5 in wild-type mice (Figure S4).

Epithelial cells in the collecting ducts are highly polarized and contain distinct apical, lateral, and basal membrane domains. Immunofluorescence staining of collecting ducts for the cell polarity marker aPKC revealed that while all wild-type tubes displayed apical localization of aPKC, many tubes in *Dlg5*$^{-/-}$ kidneys show loss of apical localization of aPKC, suggesting early defects in cell polarity (Figures 2G and 2G′). In addition, dilated collecting ducts in *Dlg5*$^{-/-}$ kidneys failed to express the apical membrane marker Aquaporin-2 (Figures 2F and 2J; Figure S5). Immunostaining for the lateral membrane marker E-cadherin revealed the presence of a distinct lateral membrane domain in *Dlg5*$^{-/-}$ cells; however, E-cadherin staining was disorganized and appeared to be more diffuse in mutant cells (Figures 2G and 2G′). Formation of renal cysts may result from abnormalities in primary cilia, representing extensions of the apical membrane domain (Zhang et al., 2004). Immunostaining with anti-acetylated-tubulin antibodies (cilia marker) revealed that, while cilia were present on *Dlg5*$^{-/-}$ cells lining nondilated tubes, they were missing on cells lining dilated tubes and cyst-like structures (Figures 2H–2I). We concluded that loss of cell polarity and the subsequent loss of cilia are the

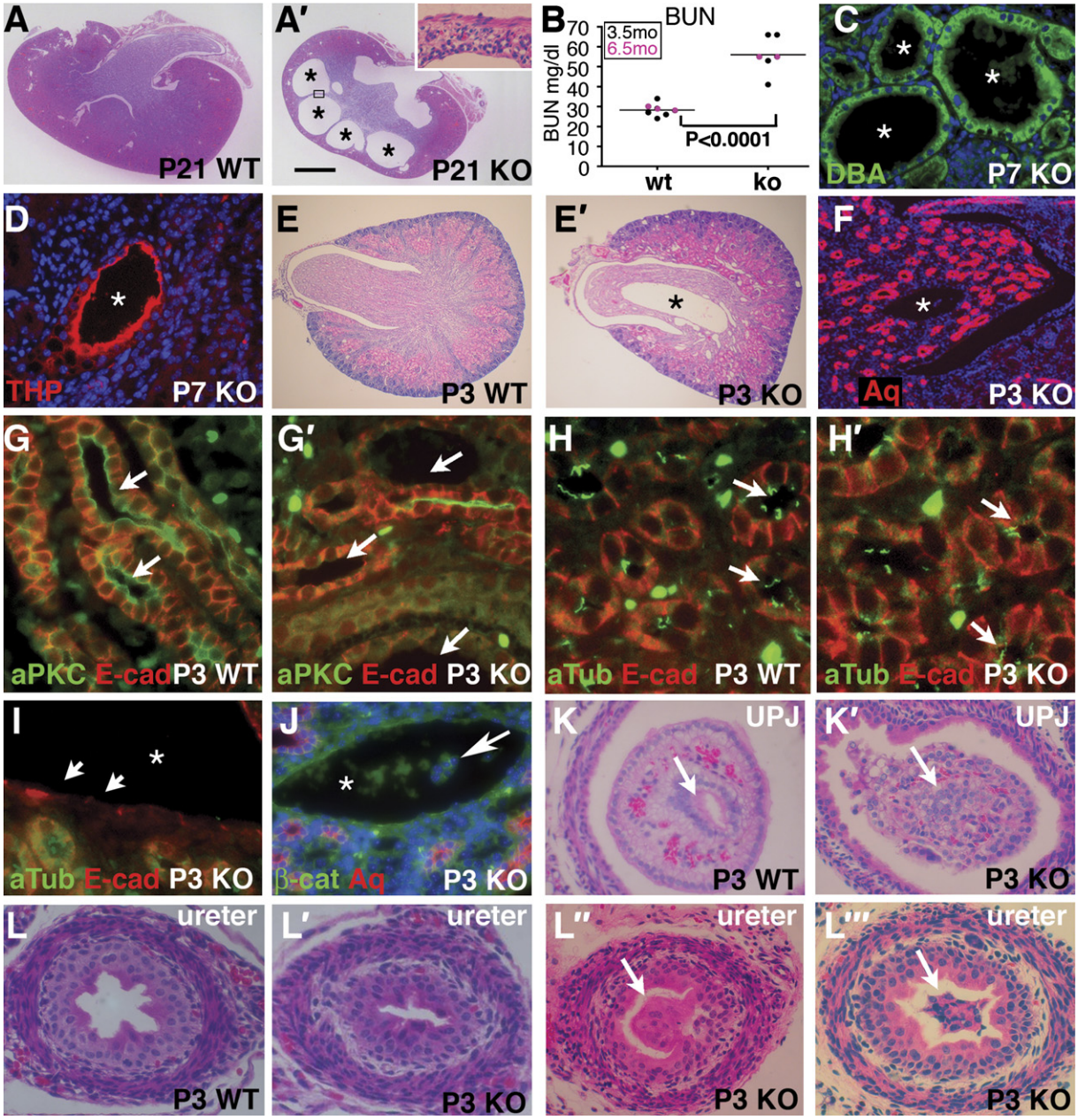

Figure 2. Loss of Cell Polarity and Renal Cysts in *Dlg5*$^{-/-}$ Mice

(A and A′) H&E staining of kidneys from P21 wild-type (WT) and *Dlg5*$^{-/-}$ (KO) mice. Note the multiple cysts (asterisks) in the mutant kidney. The inset in (A′) shows the boxed area in high magnification.

(B) Blood urea nitrogen (BUN) of 3.5- and 6.5-month-old mutant (ko) and wild-type (wt) mice. The p value was determined by a t test.

(C and D) Immunostaining of P7 early kidney cysts with DBA, a marker of collecting ducts, and THP, a marker of distal ascending tubules. Only $\leq$2% of cysts were positive for THP.

(E and E′) H&E staining of kidneys from P3 wild-type (WT) and *Dlg5*$^{-/-}$ (KO) mice. Note the developing cysts in the kidney pelvis (asterisk).

(F) Immunostaining of *Dlg5*$^{-/-}$ P3 kidney with anti-Aquaporin-2 (Aq) antibodies. Note the loss of Aquaporin-2 in the small cyst (asterisk).

(G and G′) Immunostaining of collecting ducts from wild-type (WT) and *Dlg5*$^{-/-}$ (KO) kidneys with anti-aPKC and anti-E-cadherin (E-cad) antibodies.

(H–I) Immunostaining of collecting ducts from wild-type (WT) and *Dlg5*$^{-/-}$ (KO) kidneys with anti-acetylated tubulin (aTub, cilia marker) and anti-E-cadherin (E-cad) antibodies. (I) Note the loss of tubulin staining in the cyst (asterisk, arrow).

(J) Immunostaining of a kidney from *Dlg5*$^{-/-}$ mice with anti-β-catenin (β-cat) and anti-Aquaporin-2 (Aq) antibodies. The arrow points to loss of cells into the lumen of a small cyst (asterisk).

(K–L‴) H&E staining of ureteropelvic junctions (UPJs) and ureters from P3 wild-type (WT) and *Dlg5*$^{-/-}$ (KO) mice. Note the (K′) disorganization and partial fusion of the collecting duct in UPJ, (L′) constriction of the ureter, and (L″–L‴) ureteral polyps in *Dlg5*$^{-/-}$ mice.

The scale bar in (A′) represents 1 mm in (A) and (A′), 0.4 mm in (E) and (E′), 150 μm in (F), 100 μm in (C), (D), and (K–L‴), and 40 μm in (G)–(J).

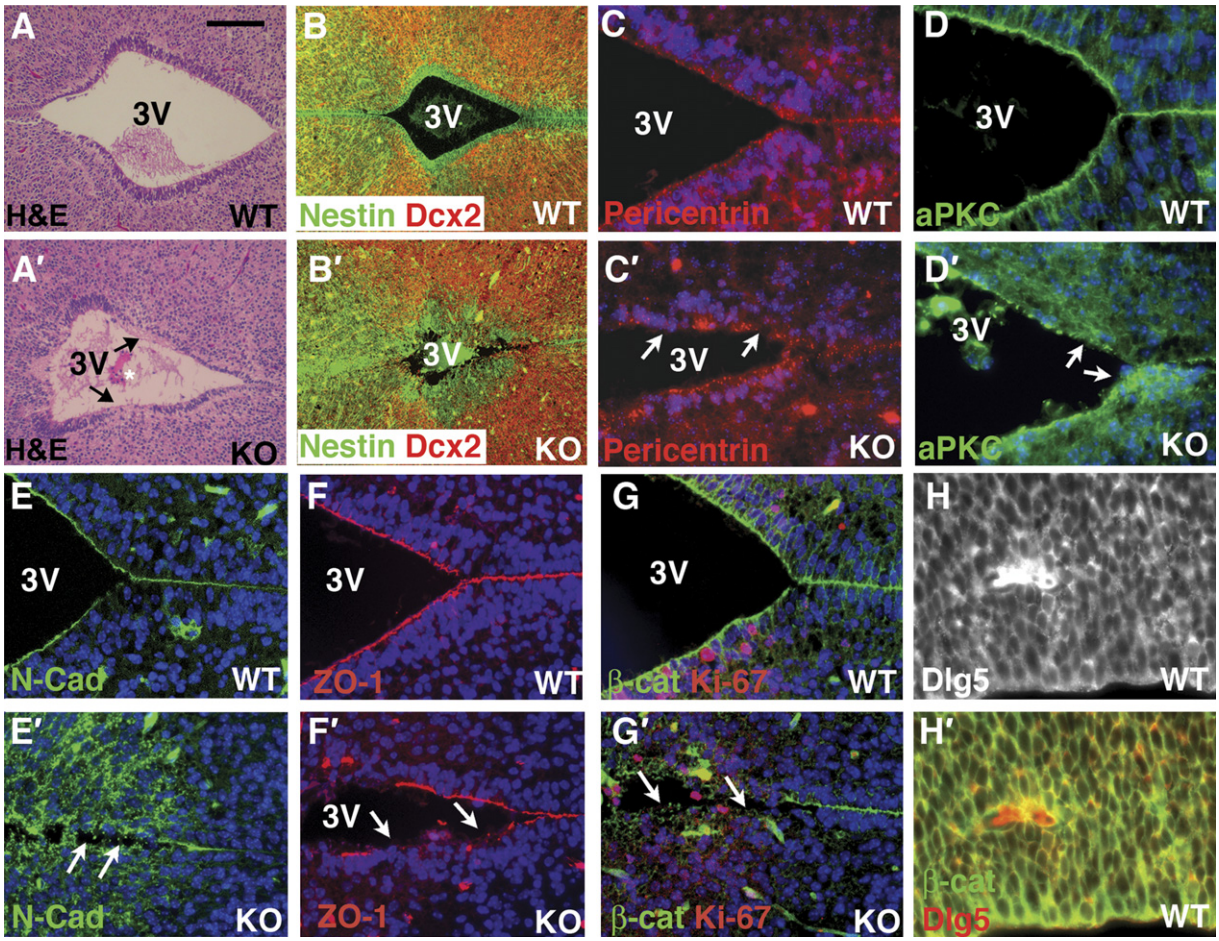

Figure 3. Disruption of Adherens Junctions and Loss of Cell Polarity as the Cellular Basis of the Epithelial Tube Maintenance Defect, Closure of the Aqueduct, and Hydrocephalus in *Dlg5*$^{-/-}$ Brains

(A–G′) Coronal sections from E15.5 *Dlg5*$^{-/-}$ (KO) and wild-type (WT) brains at the level of the third ventricle stained with (A and A′) H&E or the following antibodies: (B and B′) anti-Nestin (neural progenitor cell marker) and anti-Dcx2 (newly born neurons); (C and C′) anti-pericentrin (cilia basal body and centrosomal cell polarity marker); (D and D′) anti-aPKC (apical membrane cell polarity marker); (E and E′) anti-N-cadherin (N-cad, AJ marker); (F and F′) anti-ZO-1 (tight and AJ marker); (G and G′) anti-β-catenin (β-cat, AJ marker) and anti-Ki-67 (proliferating cell marker). Note loss of cell polarity and mislocalization of AJ proteins in *Dlg5*$^{-/-}$ progenitors (arrows).

(H and H′) Coronal brain section from the E13.5 wild-type brain stained with (H) anti-Dlg5 and (H′) anti-Dlg5 and anti-β-catenin antibodies. Staining patterns and corresponding antibodies are color-coded.

The scale bar in (A) represents 100 μm in (A)–(A′), 300 μm in (B) and (B′), 60 μm in (C)–(G′), and 40 μm in (H) and (H′).

earliest detectable defects that coincide with or precede the formation of epithelial cysts in *Dlg5*$^{-/-}$ mice.

To reveal additional defects in kidneys of *Dlg5*$^{-/-}$ mice, we performed cross-sections through the kidney pelvic region, the ureteropelvic junction (UPJ), and the ureter. In contrast to well-organized and open kidney pelvis papillary ducts at the UPJs in wild-type mice, papillary ducts in *Dlg5*$^{-/-}$ kidneys were disorganized and often failed to maintain tube openings (Figures 2K and 2K′, two out of six mice). In addition, *Dlg5*$^{-/-}$ ureters displayed constriction (four out of six mice) and formation of ureteral polyps (two out of six mice) (Figures 2L–2L‴). These abnormalities may result in the partial obstruction of the flow of urine in *Dlg5*$^{-/-}$ kidneys and contribute to renal cyst formation in *Dlg5*$^{-/-}$ mice. Therefore, in addition to classic polycystic kidney defects, *Dlg5*$^{-/-}$ kidneys showed occasional occlusion of collecting ducts, constriction of the ureter, and formation of ureteral polyps (Figures 2K–2L‴). These abnormalities are characteristic of congenital obstructive hydronephrosis. The presence of a combination of abnormalities characteristic of both polycystic kidney disease and hydronephrosis may be a unique hallmark of *Dlg5*$^{-/-}$ kidneys.

Loss of Cell Polarity and Disorganization of Apical Junctional Adhesion Complexes in *Dlg5*$^{-/-}$ Neural Progenitors

Similar to kidney collecting ducts, brain ventricular surfaces are lined with highly polarized cells. These cells are organized as pseudostratified epithelium, contain cilia at the apical membrane domain, and form prominent apical junctional adhesion complexes at the ventricular surface (Chenn et al., 1998). To determine whether loss

of cell polarity in *Dlg5*$^{-/-}$ neural progenitors may be responsible for closure of the aqueduct, we analyzed this area of the brain early in development. While *Dlg5*$^{-/-}$ progenitors from embryonic day 13.5 (E13.5) brains were undistinguishable from their wild-type counterparts, progenitors in E15.5 mice were disorganized and failed to form a polarized epithelial layer (Figures 3A–3B′). Staining with the cell polarity markers pericentrin (centrosomal and cilia basal body marker) and aPKC (apical membrane marker) revealed loss of polarity in *Dlg5*$^{-/-}$ progenitor cells (Figures 3C–3D′). In addition, while the apical junctional complex proteins N-cadherin, β-catenin, and ZO-1 were localized at the ventricular surface of the wild-type progenitors, these proteins were mislocalized in *Dlg5*$^{-/-}$ cells (Figures 3E–3G′). Instead of accumulating at the ventricular surface, the adherens junction (AJ) protein N-cadherin displayed punctate cytoplasmic localization in *Dlg5*$^{-/-}$ progenitors (Figure 3E′). Defects in epithelial layer maintenance, polarity, and adhesion in embryonic *Dlg5*$^{-/-}$ progenitors were found primarily around the third ventricle and the future aqueduct region, and they were not as prominent in other regions of the brain. This selectivity can be at least partially explained by the prominent expression of Dlg5 in areas of the third ventricle and aqueduct in wild-type mice (Figure S4).

Defects in localization of AJ proteins in *Dlg5*$^{-/-}$ cells were potentially interesting because disruption of AJs in the embryonic brain can lead to loss of polarity and disorganization of neural progenitors (Lien et al., 2006). We found that Dlg5 colocalized with β-catenin in neural progenitor cells in vivo (Figures 3H and 3H′). In addition, GFP-tagged E-cadherin and Strawberry-tagged Dlg5 colocalize at the AJs in stably transfected mammalian MDCK cells (Figure S6). Therefore, we hypothesized that Dlg5 was necessary for proper localization of AJ proteins, and loss of Dlg5 could have resulted in disorganization of AJs and a subsequent loss of polarity, cell adhesion, and, ultimately, failure of epithelial tube maintenance.

Impaired Cadherin-Catenin Complex Formation and Decreased Cell-Surface Levels of N-Cadherin in *Dlg5*$^{-/-}$ Progenitor Cells

Since immunostaining revealed mislocalization of AJ proteins in *Dlg5*$^{-/-}$ brains, we used a biochemical approach to analyze the subcellular distribution of N-cadherin and β-catenin in more detail. To determine whether N-cadherin is properly localized at the cell surface in *Dlg5*$^{-/-}$ cells, we analyzed the cell-surface levels of N-cadherin in *Dlg5*$^{-/-}$ progenitors. We found that, despite overall similar levels of N-cadherin in wild-type and mutant cells, cell-surface levels of N-cadherin and β-catenin, associated with N-cadherin, were significantly reduced in *Dlg5*$^{-/-}$ progenitors (Figures 4A and A′). We conclude that Dlg5 is necessary for cell-surface stabilization of the cadherin-catenin protein complex in neural progenitor cells. Remarkably, these changes were not restricted to progenitors around the third ventricle, but they were seen in total brain neural progenitors, suggesting that the proper localization of the cadherin-catenin complex is a general function of Dlg5.

We next analyzed whether Dlg5 is necessary for the integrity of AJs. Coimmunoprecipitation experiments reveal decreased levels of N-cadherin and α-catenin in the cadherin-catenin complexes immunoprecipitated from *Dlg5*$^{-/-}$ brains with anti-β-catenin antibodies (Figures 4B and 4B′). In addition, coimmunoprecipitation experiments indicate that Dlg5 physically interacts with β-catenin in the wild-type brain (Figure 4B). We found two β-catenin-binding sites in Dlg5: in its N-terminal and PDZ3-PDZ4 domains (Figures 4C–4E). Dlg5 was interacting not only with β-catenin, but also with cadherin, revealing the existence of cadherin-β-catenin-Dlg5 protein complexes (Figure S7).

The coiled-coil domain of Dlg5 is a unique feature that distinguishes it from all other Dlg family members. Self-association is one of the potential functions of the coiled-coil domains. To determine whether Dlg5 can self-associate, we performed coimmunoprecipitation experiments with a variety of tagged Dlg5 proteins. Dlg5 displayed prominent self-association, and subsequent experiments revealed that the N-terminal part containing the coiled-coil domain was primarily responsible for this function (Figure 5). In addition, PDZ3-PDZ4 and SH3-GUK domains of Dlg5 also displayed self-association abilities and were able to bind to the N-terminal part of Dlg5, indicating an additional possibility of a head-to-tail oligomerization or intramolecular interaction of the N terminus with the C terminus of the protein. Self-association of Dlg5 could result in the formation of large protein complexes containing multiple β-catenin-binding domains that can scaffold and stabilize cadherin-catenin complexes at the plasma membrane.

Impaired Cell-Surface Delivery and Stabilization of the N-Cadherin-Catenin Complex in *Dlg5*$^{-/-}$ MEF Cells

To investigate the mechanism of Dlg5 function responsible for localization of cadherin-catenin complexes to the AJ, we utilized primary mouse embryonic fibroblasts (MEFs). Similar to neural progenitor cells, MEFs depend on N-cadherin to form AJs (Teng et al., 2005). We found that *Dlg5*$^{-/-}$ MEFs also exhibited significantly reduced levels of cell-surface N-cadherin (Figures 6A and 6A′) and displayed decreased junctional localization of the AJ proteins N-cadherin, β-catenin, and p120-catenin (Figure S8). Reduced levels of cell-surface N-cadherin can result from deficient delivery or stabilization of the protein at the plasma membrane. To determine which of these functions was impaired in *Dlg5*$^{-/-}$ MEFs, we performed pulse-chase experiments to analyze the dynamics of cell-surface appearance and retention of ^{35}S-labeled N-cadherin (Davis et al., 2003; Teng et al., 2005). The levels and dynamics of the cell-surface appearance of N-cadherin in *Dlg5*$^{-/-}$ MEFs revealed defects in both delivery and stabilization of the protein at the plasma membrane (Figures 6B and 6B′, n = 4). We conclude that Dlg5 is necessary for cell-surface delivery and stabilization of cadherin-catenin complexes.

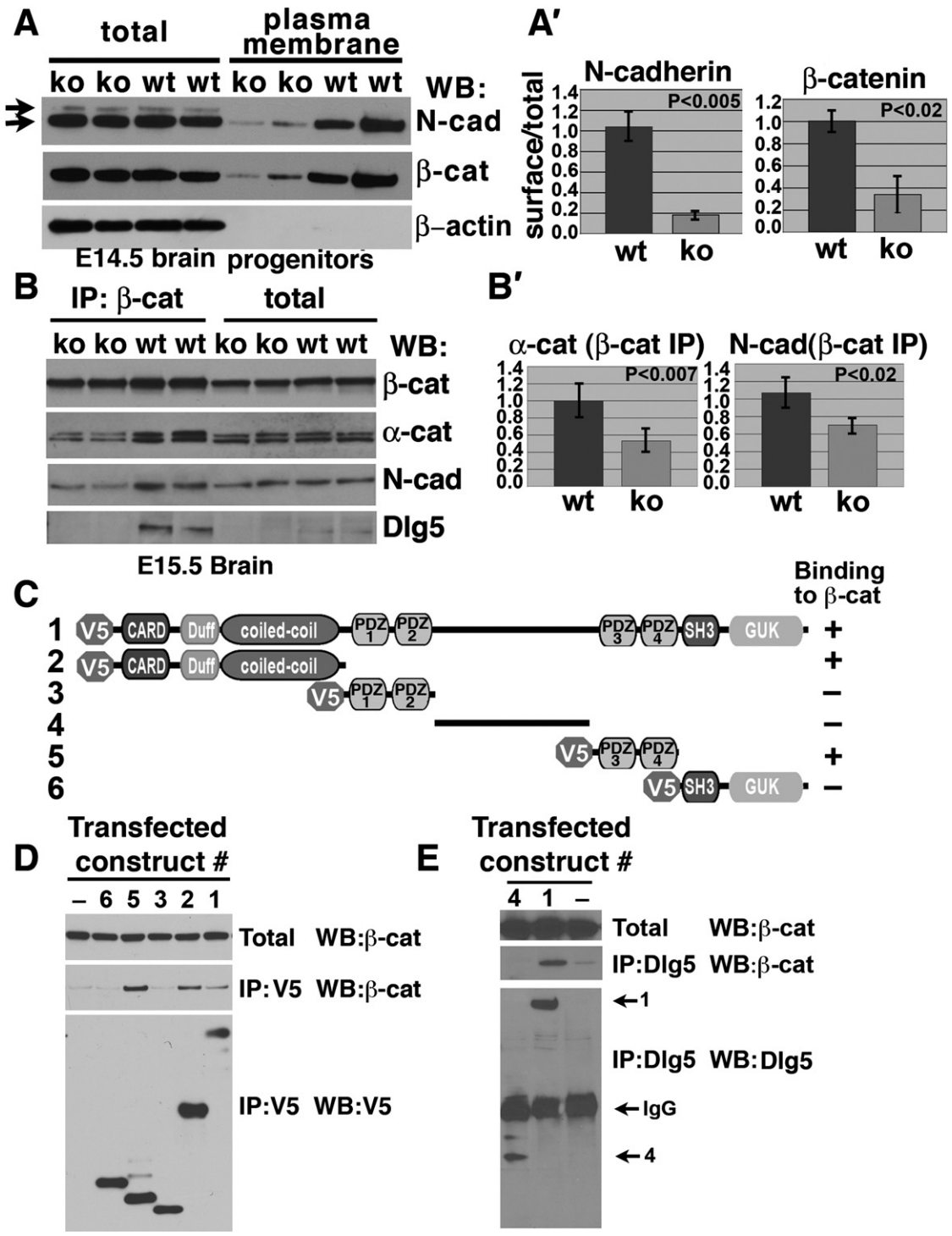

Figure 4. Decrease in Cell-Surface Levels and Destabilization of AJ Protein Complexes in *Dlg5*$^{-/-}$ Progenitors

(A) Decrease in plasma membrane-associated levels of AJ proteins in *Dlg5*$^{-/-}$ neural progenitors. Cell-surface proteins on isolated *Dlg5*$^{-/-}$ (ko) and wild-type (wt) progenitors were biotinylated, immunoprecipitated with streptavidin-Sepharose, and analyzed by blot (WB) with anti-N-cadherin (N-cad), anti-β-catenin (β-cat), and anti-β-actin antibodies. Note the similar levels of total, but decreased levels of cell-surface N-cadherin and N-cadherin-associated β-catenin, proteins. Arrows point to the precursor and processed N-cadherin. Note the absence of the precursor and β-actin in streptavidin pull-downs.

(A′) Quantitation of experiments similar to the one shown in (A). Ratios of plasma membrane to total levels of N-cadherin and β-catenin in wild-type cells arbitrarily assumed as 1 ± standard error (n = 3). The p value was determined by using an ANOVA test.

Dlg5 Localizes to AJs and N-Cadherin-Containing Vesicles and Facilitates Delivery of N-Cadherin to the AJs in Live MEFs

In normal cells, newly synthesized N-cadherin quickly associates with β-catenin and is delivered from the Golgi to the plasma membrane via secretory vesicles (Mary et al., 2002). To analyze the dynamics of Dlg5 and N-cadherin in live cells, we electroporated wild-type and *Dlg5*$^{-/-}$ MEFs with N-cadherin-GFP and Strawberry-Dlg5 expression constructs. We found that 20 hr postelectroporation, N-cadherin-GFP was localizing to the cytoplasmic vesicles and the AJs in wild-type MEFs (Figures 6C–6E″, green). Interestingly, Strawberry-Dlg5 also showed vesicular and, to a lower degree, AJ localization that significantly, but not completely, overlapped with N-cadherin-GFP (Figures 6C–6E″, red). Remarkably, while the majority of the wild-type cells electroporated with N-cadherin-GFP (89%) displayed the protein at the AJs at 20 hr after transfection, only half (49%) of the *Dlg5*$^{-/-}$ MEFs showed junctional N-cadherin-GFP (Figures 6G–6H). The majority of N-cadherin-GFP in mutant cells was localized to the cytoplasmic perinuclear vesicles. Simultaneous electroporation of *Dlg5*$^{-/-}$ MEFs with N-cadherin-GFP and Strawberry-Dlg5 constructs partially rescued this defect (Figures 6F, 6G″, and 6H). To determine the identity of Dlg5-positive vesicles, we stained MEFs and MDCK cells with a series of vesicle markers, including Rab-11, a marker of recycling endosomes; Rab-8, a marker of trans-Golgi vesicles; Rab-5 and EEA1, early endosomal markers; and GM130, a Golgi marker. While Dlg5-containing vesicles were negative for Rab-5, Rab-8, EEA1, and GM130 (data not shown), we found partial overlap between Rab-11- and Dlg5-positive vesicles (Figure S9). Interestingly, cadherin-carrying transport vesicles fuse with Rab-11-positive endosomes on their route to the plasma membrane (Lock and Stow, 2005). We conclude that Dlg5 accompanies newly synthesized N-cadherin as it is transported from the Golgi to the plasma membrane.

Dlg5 Binds to Syntaxin 4 and May Facilitate Targeted Cadherin Delivery by Linking Cadherin-Catenin-Carrying Transport Vesicles with the t-SNARE Complex at the Plasma Membrane

Efficient and targeted delivery of N-cadherin requires tethering and a SNARE-dependent fusion of N-cadherin-β-catenin-containing vesicles with the AJs. We hypothesized that Dlg5 may facilitate targeted membrane delivery of the cadherin-catenin complex by interacting with the SNARE membrane fusion machinery. We analyzed potential interactions between Dlg5 and SNARE proteins and found that endogenous Dlg5 in brains and kidneys physically associates with syntaxin 4 (Figures 7A and 7B), a t-SNARE protein responsible for vesicle delivery to the basolateral membrane domain (ter Beest et al., 2005). This interaction was specific for syntaxin 4, as we found no binding between Dlg5 and syntaxins 2 and 3 (data not shown). Syntaxin 4 colocalized with Dlg5 on cytoplasmic vesicles and AJs (Figures 7D–7E‴). Cotransfection experiments with full-length and truncated fragments of Dlg5 revealed that PDZ1-PDZ2 and PDZ3-PDZ4 domains of Dlg5 are involved in the interaction with syntaxin 4 (Figure 7C; Figure S10). It is likely that these domains have a redundant function, because deletion of either PDZ1-PDZ2 or PDZ3-PDZ4 domains was not sufficient for generation of the nonfunctional protein (Figure S11).

To summarize, we propose that Dlg5 utilizes its multiple β-catenin- and syntaxin 4-binding domains to link cadherin-carrying transport vesicles to the t-SNARE vesicle targeting complex at the lateral membrane domain of polarized cells (Figure 7F). In addition, it can potentially use its self-association and β-catenin-binding regions to cluster and stabilize cadherin-catenin complexes at the AJs. These mechanisms can ensure targeted delivery and stabilization of cadherin-catenin complexes to maintain polarity of cells forming epithelial tubes.

DISCUSSION

Maintenance of Cell Polarity by Targeted Plasma Membrane Delivery and Stabilization of the Cadherin-Catenin Complex Is a Critical Function of Dlg5

Dlg5 is a member of the MAGUK family of proteins. These molecules, especially the Dlgs, have been implicated in regulation of membrane protein targeting. Mammalian Dlg1/SAP97 and Dlg4/PSD-95 are involved in synaptic membrane clustering of AMPA receptors and ion channel proteins (Cai et al., 2006; Tiffany et al., 2000). While *Dlg2/PSD-93*$^{-/-}$ mice do not show avert abnormalities, *Dlg4/PSD-95*$^{-/-}$ mice are live and fertile, but show learning disabilities due to changes in synaptic transmission (McGee et al., 2001; Migaud et al., 1998). Mice with truncation of *Dlg1* display craniofacial malformations (Caruana and Bernstein, 2001), and *Dlg1*$^{-/-}$ animals show misorientation of smooth muscle cells in the ureter (Mahoney et al., 2006). Dlg5 is a unique MAGUK protein. While it shares many structural features with Dlg family proteins, it contains a unique N terminus carrying the coiled-coil, Duff, and CARD domains. Similar to other Dlgs, Dlg5 facilitates membrane protein targeting. However, instead of

(B) Destabilization of AJ complexes in *Dlg5*$^{-/-}$ brains. Total protein extracts from E15.5 *Dlg5*$^{-/-}$ (ko) and wild-type (wt) brains were immunoprecipitated (IP) with anti-β-catenin (β-cat) antibodies and blotted (WB) with anti-β-catenin, anti-α-catenin (α-cat), anti-N-cadherin (N-cad), and anti-Dlg5 antibodies.

(B′) Quantitation of experiments similar to the one shown in (B). Levels of α-catenin and N-cadherin in β-catenin IPs from wild-type extracts arbitrarily assumed as 1 ± standard deviation (n = 4). The p value was determined by using an ANOVA test.

(C–E) Identification of Dlg5 domains involved in binding to β-catenin. (C) Dlg5 constructs used in immunoprecipitation experiments in (D) and (E) and summary of binding results. (D and E) Indicated Dlg5 constructs were transfected into HEK293 cells, and proteins were immunoprecipitated (IP) with (D) anti-V5 or anti-Dlg5 antibodies directed against part of (E) construct #4 and analyzed by blotting (WB) with anti-V5 anti-β-catenin (β-cat) or anti-Dlg5 antibodies.

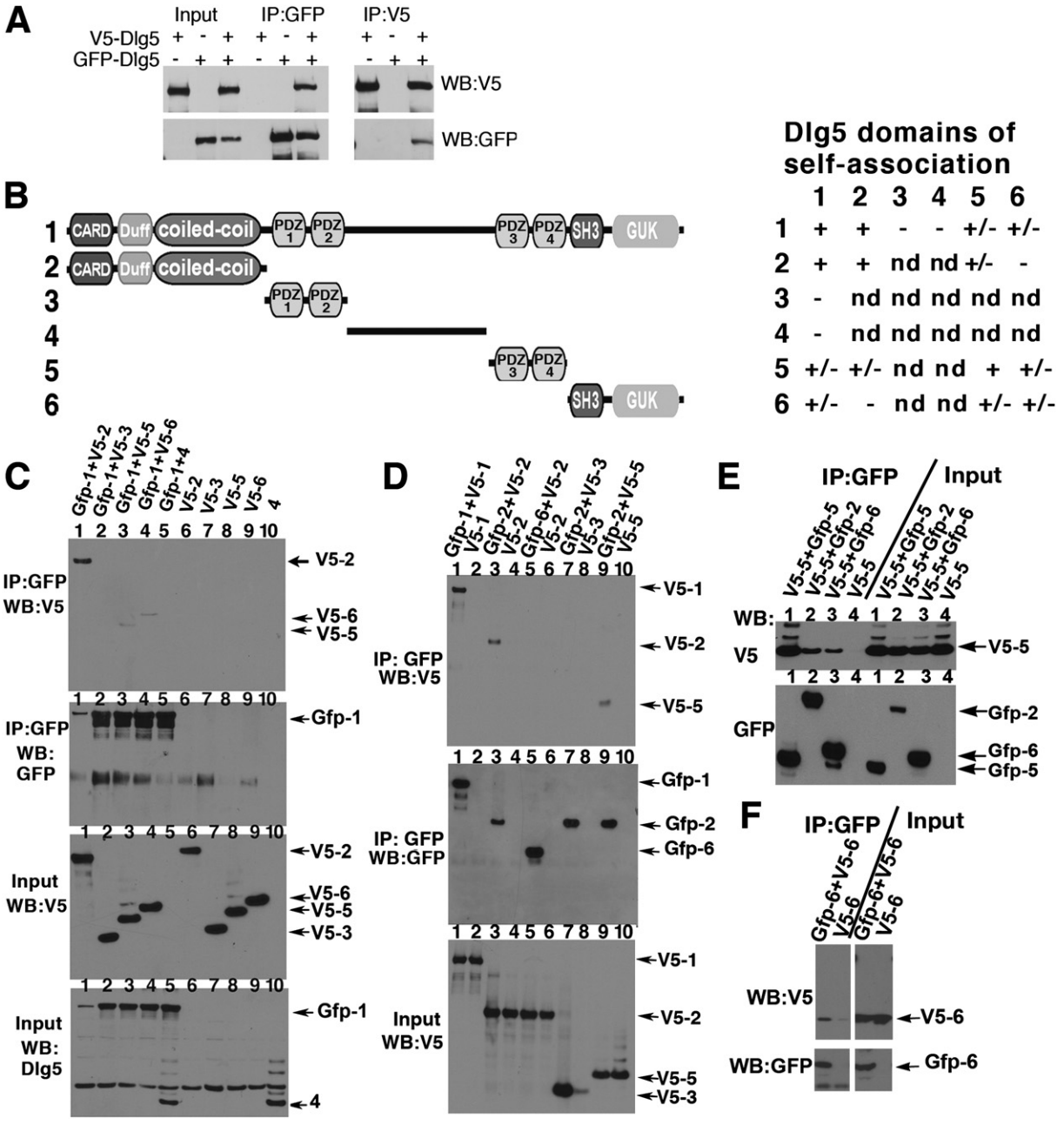

Figure 5. Self-Association of Dlg5 and Identification of Dlg5 Domains Responsible for Self-Association

(A) Self-association of full-length Dlg5. Constructs encoding GFP or V5-tagged Dlg5 proteins were cotransfected into HEK293 cells. The proteins were immunoprecipitated (IP) with anti-V5 or anti-GFP antibodies and were analyzed by western blot (WB) with anti-GFP or anti-V5 antibodies.

(B) Schematic representation of Dlg5 constructs and a summary of binding results. "ND" indicates "not determined."

(C–F) Indicated V5-tagged full-length Dlg5 or its fragments were cotransfected with GFP-tagged full-length Dlg5 or its fragments, immunoprecipitated (IP) with anti-GFP antibodies, and analyzed by western blot (WB) with anti-V5, anti-GFP, and anti-Dlg5 antibodies. Protein tags are as shown. Construct #4, without tag, was revealed by blotting with anti-Dlg5 antibody. The identity of Dlg5 constructs is encoded by the construct number shown in (B). (C) Interaction between full-length Dlg5 and its fragments. Note the strong binding of the N-terminal part of Dlg5 containing the coiled-coiled domain (V5-2) and a weaker binding of PDZ3-PDZ4 (V5-5) and SH3-GUK domains of Dlg5 (V5-6). (D) Interaction between the N-terminal part of Dlg5 (Gfp-2 or V5-2) and other Dlg5 fragments that bind to full-length Dlg5. Note the self-association of the N-terminal part of Dlg5 (V5-2 and Gfp-2) and binding to PDZ3-PDZ4 (V5-5). (E) Interaction between the PDZ3-PDZ4 domains of Dlg5 (V5-5, Gfp-5) and other Dlg5 fragments that bind to full-length Dlg5. Note the self-association of the PDZ3-PDZ4 domains of Dlg5 (V5-5 and Gfp-5) as well as its binding to the N-terminal part of Dlg5 (Gfp-2) and the C-terminal SH3-GUK domains (Gfp-6). (F) Self-association of the C-terminal SH3-GUK domain of Dlg5 (Gfp-6 and V5-6).

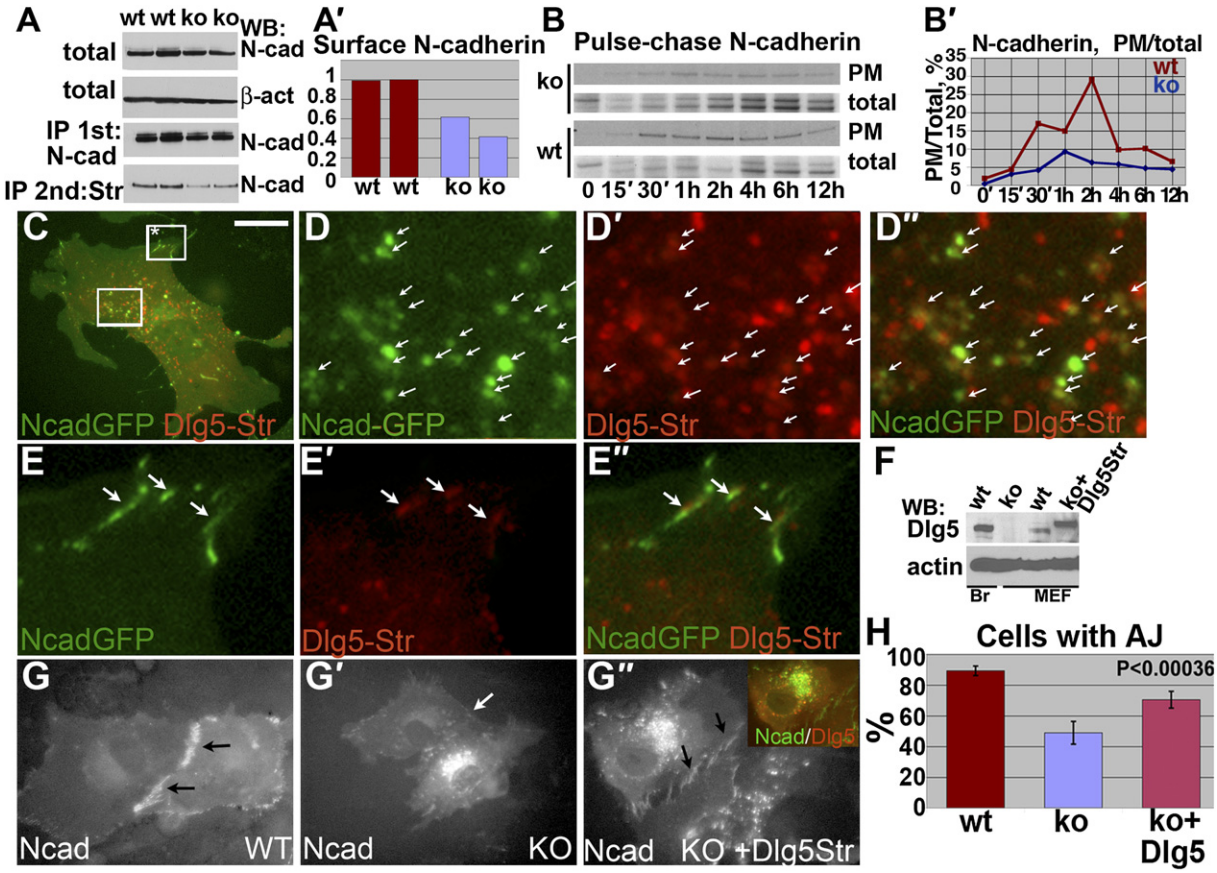

Figure 6. Dlg5 Associates with Cadherin-Carrying Transport Vesicles, and it Is Necessary for Membrane Delivery and Stabilization of Cadherin-Catenin Complexes

(A) Decreased levels of cell-surface N-cadherin in *Dlg5*$^{-/-}$ MEFs. Total proteins from cell-surface biotinylated MEFs were sequentially immunoprecipitated (IP) with anti-N-cadherin antibodies and streptavidin beads and were analyzed by immunoblotting with anti-N-cadherin (N-cad) antibodies.

(A′) Quantitation of the experiment shown in (A). Ratios of cell-surface to total N-cadherin in wild-type cells arbitrarily assumed as 1.

(B) Decrease in cell-surface delivery and stabilization of N-cadherin in *Dlg5*$^{-/-}$ MEFs. Pulse-chase analysis of cell-surface ^{35}S-methionine/cysteine-labeled N-cadherin.

(B′) Quantitation of the experiment shown in (B). The graph displays the ratios of surface to total levels of ^{35}S-labeled N-cadherin in wild-type (wt) and knockout (ko) cells at different time points.

(C–E″) Dlg5 colocalizes with newly synthesized N-cadherin on the cytoplasmic vesicles and at the AJs in live MEFs. Wild-type MEFs were electroporated with N-cadherin-GFP (N-cad-GFP, green) and Strawberry-Dlg5 (Dlg5Str, red) constructs. Localization of GFP and Strawberry proteins was detected by live-cell microscopy. Areas in boxes in (C) that contain transport vesicles (lower box) and AJs (upper box) are shown at a higher magnification in (D)–(D″) and (E)–(E″), respectively. White arrows denote colocalization between N-cadherin and Dlg5 proteins.

(F) Total protein extracts from wild-type (wt) brain (Br), *Dlg5*$^{-/-}$ (ko) and wild-type (wt) MEFs, and *Dlg5*$^{-/-}$ MEFs electroporated with the Strawberry-Dlg5 expression construct (ko+Dlg5) were analyzed by blotting with anti-Dlg5 and anti-β-actin antibodies.

(G–G″) Wild-type (WT) and *Dlg5*$^{-/-}$ (KO) MEFs were electroporated with (G and G′) N-cadherin-GFP or (G″) N-cadherin-GFP and Strawberry-Dlg5 constructs and imaged for GFP and Strawberry. Note the prominent localization of N-cadherin-GFP to cell-cell junctions in (G) wild-type, but not in (G′) *Dlg5*$^{-/-}$, MEFs, and (G″) rescue of this defect in *Dlg5*$^{-/-}$ MEFs cotransfected with Strawberry-Dlg5.

(H) Quantitation of experiments shown in (G)–(G″). The percentage of transfected cells (n = 60–110) showing junctional staining for N-cadherin-GFP was quantified, and statistical significance was determined by ANOVA analysis.

The scale bar in (C) represents 10 μm in (C), 8 μm in (G)–(G″), and 2 μm in (D)–(E″).

targeting and clustering the synaptic proteins, Dlg5 function is more general, as it is necessary for targeting and retention of the cadherin-catenin adhesion complex in many different cell types. Since the mechanisms responsible for the function of classic mammalian Dlgs (PSD-95, PSD-93, SAP-102) in synaptic targeting are still poorly understood, it will be interesting to determine whether the interaction described here between Dlg5 and the t-SNARE transport vesicle fusion machinery represents a function conserved in other Dlg proteins.

Disorganization of Intercellular Adhesion and Loss of Cell Polarity as Causal Factors in Obstructive Hydrocephalus and Renal Cysts in *Dlg5*$^{-/-}$ Mice

Loss of cell polarity and tissue disorganization are the primary cellular defects responsible for hydrocephalus in

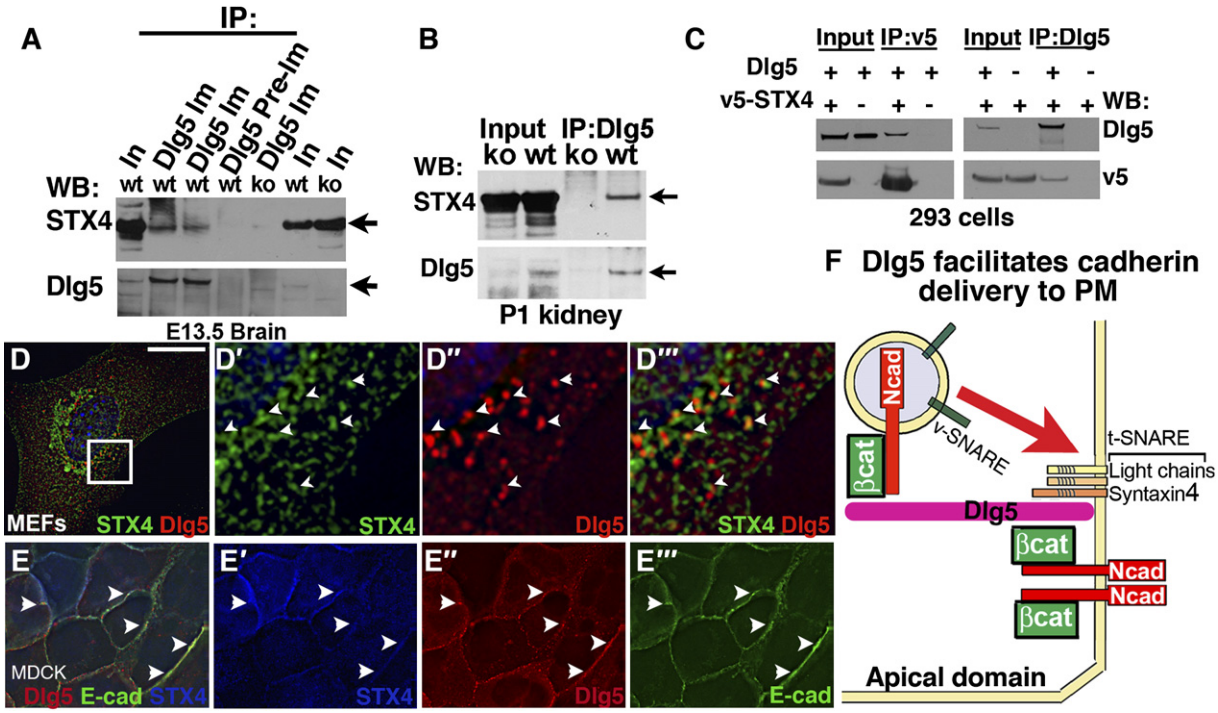

Figure 7. Interaction between Dlg5 and Syntaxin 4, a t-SNARE Protein Involved in Basolateral Vesicle Transport

(A and B) Association between endogenous Dlg5 and syntaxin 4 (STX4) proteins in (A) E13.5 brains and (B) P1 kidneys. Total protein lysates were immunoprecipitated (IP) with anti-Dlg5 immune and preimmune serum and were analyzed by blotting (WB) with anti-Dlg5 or anti-syntaxin 4 antibodies.

(C) Coimmunoprecipitation of full-length Dlg5 and syntaxin 4 proteins expressed in HEK293 cells. The Dlg5 construct was cotransfected with V5-tagged syntaxin 4 (STX4), and immunoprecipitates with anti-Dlg5 or anti-V5 antibodies were analyzed by western blot with anti-Dlg5 or anti-V5 antibodies.

(D) Colocalization of Dlg5 (red) and syntaxin 4 (green) in MEFs, electroporated with the fluorescently labeled Strawberry-Dlg5 and V5-syntaxin 4, fixed, and stained with anti-V5 antibody.

(E) Colocalization of syntaxin 4 (blue) with Dlg5 (red) and E-cadherin (green). The V5-syntaxin 4 construct was electroporated into MDCK cells stably expressing Strawberry-Dlg5 and E-cadherin-GFP; cells were fixed and stained with anti-syntaxin 4 antibody.

(F) Model of Dlg5 function in plasma membrane delivery of cadherin-catenin adhesion complexes by linking the t-SNARE vesicle targeting complex with N-cadherin/β-catenin-carrying transport vesicles.

The scale bar in (D) represents 15 μm in (D), 2 μm in (D′)–(D‴), and 25 μm in (E)–(E‴).

Dlg5$^{-/-}$ animals. Indeed, nonpolarized and disorganized progenitors in the developing *Dlg5*$^{-/-}$ brain are unable to maintain proper tube architecture and fail to keep the aqueduct open. This results in obstruction of the ventricular liquid flow and subsequent hydrocephalus. As in *Dlg5* mutants, disruption of intercellular adhesion and disorganization of neural progenitors are responsible for closure of the aqueduct and severe hydrocephalus in *myosin IIB*$^{-/-}$ mice (Tullio et al., 2001). In addition, humans and mice with mutations in cell-adhesion molecule L1 display closure of the aqueduct and hydrocephalus (Itoh et al., 2004). Mutation in αSNAP protein, a receptor for the SNARE complex involved in polarized membrane targeting, causes disruption in localization of apical junctional proteins and results in obstructive hydrocephalus (Chae et al., 2004). Overall, despite complex genetic causes of obstructive hydrocephalus, the abnormalities involving the disruption of adhesion and cell polarity of neural progenitor cells may represent a common cellular defect responsible for this devastating disease.

Cell polarity is critical for proper morphogenesis and maintenance of epithelial tubes not only in the developing brain, but also in the kidney. We found that *Dlg5*$^{-/-}$ kidneys develop dilation of collecting ducts and formation of cysts. The majority of proteins implicated in mammalian polycystic kidney disease localize to the epithelial junctions and primary cilium, and some of these proteins are also involved in hydrocephalus (Harris and Torres, 2006; Taulman et al., 2001). Primary cilium is an apical membrane extension, and cilia retention is likely to require proper maintenance of epithelial cell polarity. *Dlg5*$^{-/-}$ animals develop early defects in polarized localization of aPKC, which are followed by the loss of cilia. It is likely that disruption of cell polarity in *Dlg5*$^{-/-}$ cells affects cilia maintenance, which results in subsequent epithelial cysts formation.

In summary, we report a new gene responsible for mammalian hydrocephalus and renal cysts. We report that Dlg5 is required for the maintenance of AJs and epithelial cell polarity in mammalian brain and kidneys. At

the molecular level, Dlg5 is necessary for cell-surface delivery and stabilization of cadherin-catenin adhesion complexes. Finally, we demonstrate that Dlg5 binds to t-SNARE basolateral vesicle targeting machinery and also travels with cadherin-catenin-carrying transport vesicles. We propose that Dlg5 uses its unique N-terminal self-association domain to tether cadherin-containing transport vesicles to the t-SNARE complex to ensure polarized membrane delivery of AJ proteins.

EXPERIMENTAL PROCEDURES

Generation of *Dlg5*$^{-/-}$ Mice

The *Dlg5* null allele in ES cells was generated by using standard DNA recombination technology (Hogan, 1994). Chimeras that were generated from ES cells were crossed to C57/BL6 mice, and the resulting heterozygous animals were crossed with each other to produce the *Dlg5*$^{-/-}$ mice. Mouse genotyping was performed by PCR with the following oligos: PGKFwd2, 5′-ATTGCATCGCATTGTCTGAGTAGGTG-3′; Dlg5B11, 5′-CATGGTGCAATGCAACTTCCTC-3′; and Dlg5A14, 5′-TGCTACTGCTGCAGAGTCCTCC-3′. The wild-type allele of Dlg5 is amplified by the B11-A14 primer pair, and the knockout allele is amplified by the PGKFwd2-Dlg5B11 pair.

Immunofluorescence, Western Blot Analyses, Immunoprecipitation, and Antibodies

Immunofluorescent staining, immunoprecipitation, and western blot analysis were performed as described (Klezovitch et al., 2004). Fixed and stained, or live, cells were analyzed by using a Zeiss fluorescent microscope in 0.2 micron Z steps and were deconvoluted by using Deltavision. Antibodies used were anti-β-tubulin III, anti-β-actin, anti-GFAP, anti-S100 (Sigma), anti-nestin (Developmental Studies Hybridoma Bank), anti-Ki67 (Novocastra), anti-N-cadherin, anti-ZO1 (Zymed), anti-Rab-11, anti-Rab-5, anti-Rab-8, anti-GM130 (BD Biosciences), anti-EEA1 (AffinityBioreagents), anti-aPKC (Santa Cruz), anti-Aquaporin-2 (gift from M. Knepper), *Dolichos biflorius* agglutinin (Vector Laboratories), anti-Tamm Horstall protein (Biomedical Technologies), anti-Dcx2 (Chemicon), anti-syntaxin 4 (SYSY), and anti-V5 (Invitrogen). Anti-Dlg5 antibodies were generated in rabbits by using a GST-Dlg5 fusion containing 204 amino acids (aa) of mouse Dlg5 (aa 1139–1343, GB# AK 147699) (Proteintech Group). Antibodies were affinity purified by using sequential GST-Sepharose depletion and GST-Dlg5 affinity purification.

DNA Constructs

The coding sequence of Dlg5, syntaxin 4, and Dlg5 deletion constructs were generated by PCR, subcloned into pENTRY vector, and subsequently transferred into pDestV5 or pDest53 vectors (Invitrogen). Full-length N-cadherin was cloned into pEGFP-N1 vector to generate a C-terminal GFP fusion. The Strawberry sequence from pRSET plasmid was PCR amplified and N-terminally fused to full-length Dlg5 in the pCMVSport6 vector. All expression constructs were verified by sequencing.

Cell Culture and Biochemical Studies

Primary MEFs were isolated and maintained as described (Hogan, 1994). MEFs and HEK293 cells were maintained in DMEM media supplemented with 10% fetal bovine serum, glutamine, nonessential amino acids, and antibiotics. MEFs were electroporated by using MEF1 reagent (Amaxa). HEK293 cells were transfected by using calcium phosphate precipitation. MDCK cells stably expressing E-cadherin-EGFP were cotransfected with Strawberry-Dlg5 and pBabe (puro) vector and were clonally selected for puromycin resistance and red fluorescent Dlg5.

Steady-State and Pulse-Chase Kinetics of N-Cadherin

Primary neural progenitor cells were isolated by trypsin digestion in the presence of Ca^{2+}/Mg^{2+} to preserve transmembrane cadherins (Bonifacino, 1998; Johansson et al., 1999). Cell-surface proteins were labeled with cell-impermeable biotin (Pierce), followed by inactivation of biotin label and lysis of the cells. Biotinylated surface proteins were pulled down with streptavidin beads and analyzed by western blot. Steady-state cell-surface and total levels of N-cadherin were determined by western blot with anti-N-cadherin antibodies (Teng et al., 2005). For pulse-chase analysis of cell-surface delivery of N-cadherin, MEFs were labeled with ^{35}S-methionine/cysteine for 20 min, washed, and chased for various times prior to surface biotinylation and lysis. To obtain total and cell-surface levels of N-cadherin, sequential immunoprecipitation with anti-N-cadherin antibodies, followed by pull-down on streptavidin-Sepharose, was used as described (Davis et al., 2003). Quantitation of junctional levels of AJ proteins in MEFs was performed as described (Teng et al., 2005).

In Situ Hybridization

In situ hybridization on cryosections was performed as described (Sciavolino et al., 1997). A 919 bp *Dlg5* cDNA fragment was amplified with primers 5′-GTTCTGCAGATGCCCACTTGAGG-3′ and 5′-CGCATGAGATTCCAGAATTGTCC-3′, subcloned into a PCR-4-TOPO vector (Invitrogen), linearized, and transcribed to obtain sense and antisense RNA probes (Ambion).

BUN Analyses

Blood was collected from mice orbital sinuses and processed by the Phoenix Central Laboratory (Everett, WA).

Supplemental Data

Supplemental Data include 11 figures and a movie and are available at http://www.developmentalcell.com/cgi/content/full/13/3/338/DC1/.

ACKNOWLEDGMENTS

We thank P. Soriano, S. Parkhurst, J. Cooper, B. Helbing, and all members of the V.V. laboratory for critical reading of this manuscript; J.W. Nelson for the gift of E-cadherin-GFP-expressing MDCK cells; R.Y. Tsien for the gift of mStrawberry; M. Knepper and the Developmental Studies Hybridoma Bank for the gift of antibodies; Marino Zerial for the Rab-11-GFP construct; Nanyan Jiang for injections of embryonic stem cells; Olga Klezovitch for maintenance of *Dlg5*$^{-/-}$ mice and timed pregnancies; and Linda Cherepow for help with histology. This work was supported by R01 CA098161 and R01 CA102365 (to V.V.), and by Chromosome Metabolism and Cancer Training Grant, National Institutes of Health (NIH) T32 CA09657 and Viral Oncology Training Grant, NIH T32 CA09229 (to T.N.).

Received: February 13, 2007
Revised: July 6, 2007
Accepted: July 23, 2007
Published: September 4, 2007

REFERENCES

Bonifacino, J.S. (1998). Current Protocols in Cell Biology (New York: John Wiley).

Buning, C., Geerdts, L., Fiedler, T., Gentz, E., Pitre, G., Reuter, W., Luck, W., Buhner, S., Molnar, T., Nagy, F., et al. (2006). DLG5 variants in inflammatory bowel disease. Am. J. Gastroenterol. *101*, 786–792.

Cai, C., Li, H., Rivera, C., and Keinanen, K. (2006). Interaction between SAP97 and PSD-95, two Maguk proteins involved in synaptic trafficking of AMPA receptors. J. Biol. Chem. *281*, 4267–4273.

Caruana, G., and Bernstein, A. (2001). Craniofacial dysmorphogenesis including cleft palate in mice with an insertional mutation in the discs large gene. Mol. Cell. Biol. *21*, 1475–1483.

Chae, T.H., Kim, S., Marz, K.E., Hanson, P.I., and Walsh, C.A. (2004). The *hyh* mutation uncovers roles for α Snap in apical protein localization and control of neural cell fate. Nat. Genet. *36*, 264–270.

Chenn, A., Zhang, Y.A., Chang, B.T., and McConnell, S.K. (1998). Intrinsic polarity of mammalian neuroepithelial cells. Mol. Cell. Neurosci. *11*, 183–193.

Davis, M.A., Ireton, R.C., and Reynolds, A.B. (2003). A core function for p120-catenin in cadherin turnover. J. Cell Biol. *163*, 525–534.

Doetsch, F., Petreanu, L., Caille, I., Garcia-Verdugo, J.M., and Alvarez-Buylla, A. (2002). EGF converts transit-amplifying neurogenic precursors in the adult brain into multipotent stem cells. Neuron *36*, 1021–1034.

Garcia, A.D., Doan, N.B., Imura, T., Bush, T.G., and Sofroniew, M.V. (2004). GFAP-expressing progenitors are the principal source of constitutive neurogenesis in adult mouse forebrain. Nat. Neurosci. *7*, 1233–1241.

Harris, P.C., and Torres, V.E. (2006). Understanding pathogenic mechanisms in polycystic kidney disease provides clues for therapy. Curr. Opin. Nephrol. Hypertens. *15*, 456–463.

Hogan, B. (1994). Manipulating the Mouse Embryo: A Laboratory Manual, Second Edition (Plainview, NY: Cold Spring Harbor Laboratory Press).

Itoh, K., Cheng, L., Kamei, Y., Fushiki, S., Kamiguchi, H., Gutwein, P., Stoeck, A., Arnold, B., Altevogt, P., and Lemmon, V. (2004). Brain development in mice lacking L1–L1 homophilic adhesion. J. Cell Biol. *165*, 145–154.

Johansson, C.B., Momma, S., Clarke, D.L., Risling, M., Lendahl, U., and Frisen, J. (1999). Identification of a neural stem cell in the adult mammalian central nervous system. Cell *96*, 25–34.

Klezovitch, O., Fernandez, T.E., Tapscott, S.J., and Vasioukhin, V. (2004). Loss of cell polarity causes severe brain dysplasia in Lgl1 knockout mice. Genes Dev. *18*, 559–571.

Lendahl, U., Zimmerman, L.B., and McKay, R.D. (1990). CNS stem cells express a new class of intermediate filament protein. Cell *60*, 585–595.

Lien, W.H., Klezovitch, O., Fernandez, T.E., Delrow, J., and Vasioukhin, V. (2006). αE-catenin controls cerebral cortical size by regulating the hedgehog signaling pathway. Science *311*, 1609–1612.

Lock, J.G., and Stow, J.L. (2005). Rab11 in recycling endosomes regulates the sorting and basolateral transport of E-cadherin. Mol. Biol. Cell *16*, 1744–1755.

Lubarsky, B., and Krasnow, M.A. (2003). Tube morphogenesis: making and shaping biological tubes. Cell *112*, 19–28.

Mahoney, Z.X., Sammut, B., Xavier, R.J., Cunningham, J., Go, G., Brim, K.L., Stappenbeck, T.S., Miner, J.H., and Swat, W. (2006). Discs-large homolog 1 regulates smooth muscle orientation in the mouse ureter. Proc. Natl. Acad. Sci. USA *103*, 19872–19877.

Mary, S., Charrasse, S., Meriane, M., Comunale, F., Travo, P., Blangy, A., and Gauthier-Rouviere, C. (2002). Biogenesis of N-cadherin-dependent cell-cell contacts in living fibroblasts is a microtubule-dependent kinesin-driven mechanism. Mol. Biol. Cell *13*, 285–301.

McGee, A.W., Topinka, J.R., Hashimoto, K., Petralia, R.S., Kakizawa, S., Kauer, F.W., Aguilera-Moreno, A., Wenthold, R.J., Kano, M., and Bredt, D.S. (2001). PSD-93 knock-out mice reveal that neuronal MAGUKs are not required for development or function of parallel fiber synapses in cerebellum. J. Neurosci. *21*, 3085–3091.

Migaud, M., Charlesworth, P., Dempster, M., Webster, L.C., Watabe, A.M., Makhinson, M., He, Y., Ramsay, M.F., Morris, R.G., Morrison, J.H., et al. (1998). Enhanced long-term potentiation and impaired learning in mice with mutant postsynaptic density-95 protein. Nature *396*, 433–439.

Nakamura, H., Sudo, T., Tsuiki, H., Miyake, H., Morisaki, T., Sasaki, J., Masuko, N., Kochi, M., Ushio, Y., and Saya, H. (1998). Identification of a novel human homolog of the *Drosophila* dlg, P-dlg, specifically expressed in the gland tissues and interacting with p55. FEBS Lett. *433*, 63–67.

Page, R., and Leure-duPree, A.E. (1983). Ependymal Alterations in Hydrocephalus, *Volume 2* (New York: Plenum Press).

Sarnat, H.B. (1995). Ependymal reactions to injury. A review. J. Neuropathol. Exp. Neurol. *54*, 1–15.

Sciavolino, P.J., Abrams, E.W., Yang, L., Austenberg, L.P., Shen, M.M., and Abate-Shen, C. (1997). Tissue-specific expression of murine Nkx3.1 in the male urogenital system. Dev. Dyn. *209*, 127–138.

Spassky, N., Merkle, F.T., Flames, N., Tramontin, A.D., Garcia-Verdugo, J.M., and Alvarez-Buylla, A. (2005). Adult ependymal cells are postmitotic and are derived from radial glial cells during embryogenesis. J. Neurosci. *25*, 10–18.

Stoll, M., Corneliussen, B., Costello, C.M., Waetzig, G.H., Mellgard, B., Koch, W.A., Rosenstiel, P., Albrecht, M., Croucher, P.J., Seegert, D., et al. (2004). Genetic variation in DLG5 is associated with inflammatory bowel disease. Nat. Genet. *36*, 476–480.

Taulman, P.D., Haycraft, C.J., Balkovetz, D.F., and Yoder, B.K. (2001). Polaris, a protein involved in left-right axis patterning, localizes to basal bodies and cilia. Mol. Biol. Cell *12*, 589–599.

Teng, J., Rai, T., Tanaka, Y., Takei, Y., Nakata, T., Hirasawa, M., Kulkarni, A.B., and Hirokawa, N. (2005). The KIF3 motor transports N-cadherin and organizes the developing neuroepithelium. Nat. Cell Biol. *7*, 474–482.

ter Beest, M.B., Chapin, S.J., Avrahami, D., and Mostov, K.E. (2005). The role of syntaxins in the specificity of vesicle targeting in polarized epithelial cells. Mol. Biol. Cell *16*, 5784–5792.

Tiffany, A.M., Manganas, L.N., Kim, E., Hsueh, Y.P., Sheng, M., and Trimmer, J.S. (2000). PSD-95 and SAP97 exhibit distinct mechanisms for regulating K(+) channel surface expression and clustering. J. Cell Biol. *148*, 147–158.

Tullio, A.N., Bridgman, P.C., Tresser, N.J., Chan, C.C., Conti, M.A., Adelstein, R.S., and Hara, Y. (2001). Structural abnormalities develop in the brain after ablation of the gene encoding nonmuscle myosin II-B heavy chain. J. Comp. Neurol. *433*, 62–74.

Zhang, Q., Taulman, P.D., and Yoder, B.K. (2004). Cystic kidney diseases: all roads lead to the cilium. Physiology (Bethesda) *19*, 225–230.